Article

Hydrophobic Modification of ZrO₂-SiO₂ Xerogel and Its Adsorption Properties to Rhodamine B

Yan Liu and Jing Yang *

School of Urban Planning and Municipal Engineering, Xi'an Polytechnic University, Xi'an 710048, China
* Correspondence: 20020706@xpu.edu.cn

Abstract: Zirconium nitrate pentahydrate ($Zr(NO_3)_4 \cdot 5H_2O$) and tetraethyl orthosilicate (TEOS) are used as the zirconium source and silicon source, respectively, and methyltriethoxysilane (MTES) as the hydrophobic modifier; the hydrophilic and hydrophobic ZrO_2-SiO_2 xerogels were prepared successfully. The xerogels were characterized using Fourier transform infrared spectra (FTIR), X-ray diffraction (XRD), scanning electron microscopy (SEM), and N_2 adsorption–desorption measurement. The adsorption mechanism of hydrophobic ZrO_2-SiO_2 xerogels to RhB was described by the kinetic and adsorption isotherms. The results showed that the introduction of Si-CH_3 groups can make the average pore size, BET surface area, and total pore volume of ZrO_2-SiO_2 xerogel increase. The hydrophobic ZrO_2-SiO_2 xerogel displays an adsorption capacity of 169.23 mg·g^{-1} for RhB dye at 25 °C and pH = 3. The adsorption process of hydrophobic ZrO_2-SiO_2 xerogel to RhB followed a pseudo–second-order kinetic model. Fitting results from the D–R model of adsorption indicate that the adsorption of RhB onto the hydrophobic ZrO_2-SiO_2 xerogels is mainly physical, accompanied by a spontaneous heat absorption process. The regeneration and recycling properties of hydrophobic xerogels were investigated, and their recoverability and reusability were demonstrated.

Keywords: methyl-modified; hydrophilic; hydrophobic; adsorption; rhodamine B; kinetic; adsorption isotherms

1. Introduction

Rhodamine B (RhB) (its structure is shown in Figure 1) is a basic cationic dye that was used in large quantities as a food additive and was later banned from the food industry because of experimental evidence of its carcinogenicity. However, RhB is still widely used in laboratories, the paper industry, the textile printing and dyeing industry, colored glass, specialty fireworks, and other industries [1]. These industries produce large amounts of RhB dye wastewater, which, if not properly treated, can cause great harm to human health and the ecological environment. Thus, it is important to seek an efficient and economical method for the treatment of dye wastewater represented by RhB [2]. Furthermore, due to the continuous industrial demand for RhB and the increased difficulty in treating RhB-containing dye wastewater, there is an increasing interest in its degradation and removal [3–6]. To our knowledge, there were many treatment methods [7–11] implemented for removing the eco-toxic dyes from aqueous solutions, therein including coagulation, chemical oxidation, photodegradation, membrane filtration, and adsorption. Among these methods, adsorption was deemed to be a high-efficiency and low-cost technology for removing those hazardous impurities from aqueous solutions. The high effectiveness and wide availability of an adsorbent make it very attractive for dye removal from the water environment. By far, for its low cost and energy consumption, adsorption was frequently chosen in the separation process [12–14]. High-performance adsorption materials mainly included activated carbon, nanometallic oxide, graphene, zeolite, "Greek coffee" grounds, etc.
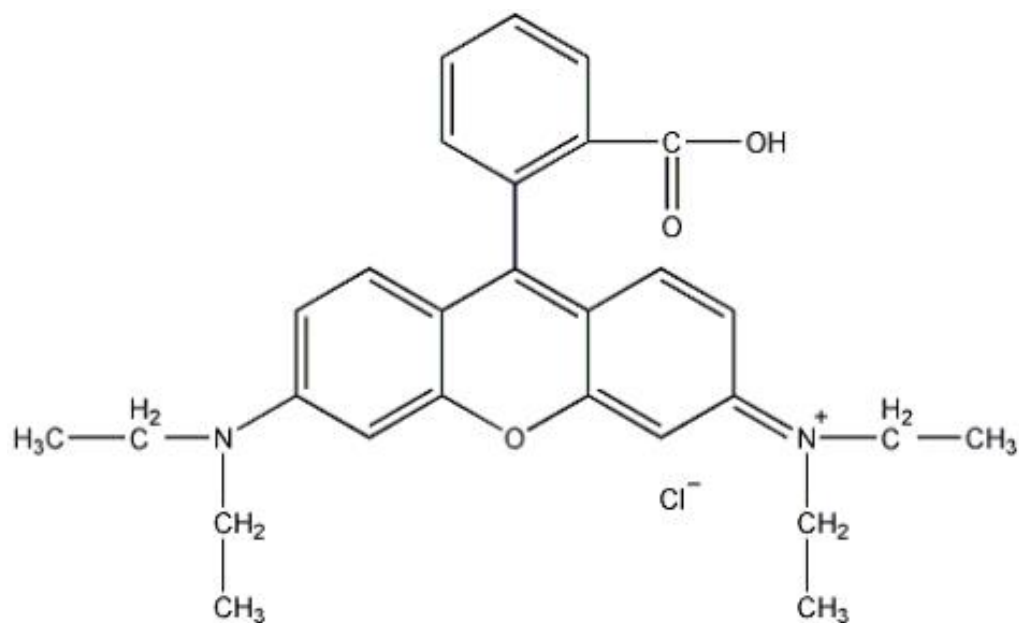
Figure 1. Molecular structural models of RhB.

Zirconia (ZrO_2), one of the important transition metal oxides, has received considerable attention for its wide applications in oxygen sensors, fuel cell electrolytes, catalysts, and catalytic carriers, and metal-oxide-semiconductor devices due to a high number of active sites on the ZrO_2 surface, good strength, large pore size, and high chemical stability, etc. [15]. The addition of metal oxides [16,17] can provide adsorption sites for the reactants and improve the adsorption performance, and also increase the anti-pollution properties. Ali et al. [18] prepared ZrO_2/CeO_2 adsorbent materials for the adsorption of acid green 1 dye using a co-precipitation method. Lin et al. [19] synthesized $ZrO_2/carbon$ aerogel (CA) composites with different amounts of monoclinic and tetragonal ZrO_2 crystallites. The adsorption capacity of ZrO_2/CA materials for cationic RhB dyes is 95.42 mg·g^{-1}. SiO_2 is a porous material with low density, good thermal stability, chemically stable properties, and excellent adsorption properties, and is widely used as a carrier xerogel for adsorption [20,21]. Shishmakov et al. [22] synthesized ZrO_2-SiO_2 xerogels through the hydrolysis of a mixture of tetrabutoxyzirconium and tetraethoxysilane in a desiccator in a vapor of a 15% aqueous NH_3 atmosphere. Viter [23] synthesized mixed oxide dry gels of ZrO_2-SiO_2 from $ZrOCl_2$-$8H_2O$ and tetraethylorthosilicate $[Si(OEt)_4]$ by the sol–gel method. The synthesized gels had a substantially increased porosity with specific surface areas of 140–630 m^2·g^{-1} and pore volumes of 0.087–0.441 cm^3·g^{-1}. Huang et al. [24] prepared a SiO_2-ZrO_2 xerogel using TEOS as a silicon source and $ZrO(NO)_3$·$2H_2O$ as Zr source. Its specific surface area reached up to 525.6 m^2·g^{-1} after 600 °C heat treatment, with an average pore size of 8.5 nm and a pore volume of 1.16 cm^3·g^{-1} and an RhB adsorption capacity of about 119 mg·g^{-1} at pH = 4 and a contact time of 4 h.

So far, studies on hydrophilic ZrO_2-SiO_2 xerogels are relatively common [25], however, when preparing ZrO_2-SiO_2 xerogels, a large amount of -OH groups are generated during the hydrolysis of TEOS, which can easily cause shrinkage or even cracking during the synthesis of composite xerogels and destroy their pore structure and affecting the adsorption performance. In this regard, the modification of hydrophilic ZrO_2-SiO_2 composite xerogels with methyl hydrophobicity is a worthwhile approach to explore. For this reason, in this paper, the hydrophobic modification was performed by introducing methyl groups based on the synthesis of hydrophilic ZrO_2-SiO_2 composite xerogels, and the characterization results of two samples and different influencing factors on the adsorption performance of RhB were compared.

For this, RhB was selected as the adsorbent and hydrophilic and hydrophobic ZrO$_2$-SiO$_2$ xerogels were prepared in this paper. The xerogels were characterized by FTIR, XRD, SEM, and N$_2$ adsorption–desorption. The adsorption performance of the hydrophilic and hydrophobic ZrO$_2$-SiO$_2$ xerogels on RhB was analyzed under the influence of different dosages, pH, and adsorption times and temperatures. In addition, the adsorption kinetics and adsorption isotherms of hydrophobic ZrO$_2$-SiO$_2$ xerogel were investigated. Prepare for the removal of more diverse dyes in the future.
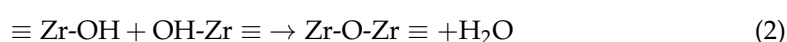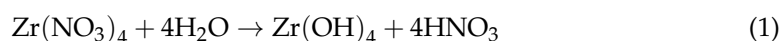
2. Experimental Section

2.1. Sol Preparation

2.1.1. Preparation of ZrO$_2$ Sol

The ZrO$_2$ sols were prepared by sol–gel method using zirconium nitrate pentahydrate (Zr(NO$_3$)$_4$·5H$_2$O, Tianjin Fuchen Chemical Reagent Co., Ltd., Tianjin, China) as the precursor and oxalic acid (C$_2$H$_2$O$_4$·2H$_2$O, p.a. grade, Tianjin Hedong Hongyan Chemical Reagent Co., Ltd., Tianjin, China) as the solvent. A certain amount of Zr(NO$_3$)$_4$ solution was added to the three-mouth flask, and 0.2 mol·L^{-1} of C$_2$H$_2$O$_4$ solution was added to the Zr (NO$_3$)$_4$ solution drop by drop with the volume ratio of Zr(NO$_3$)$_4$/C$_2$H$_2$O$_4$ = 3/2. After the temperature of the water bath reached 50 °C, 30% (*v/v*) of propanetriol (GL, p.a. grade, Tianjin Kemiou Chemical Reagent Co., Ltd., Tianjin, China) was added drop by drop and stirred strongly for 3 h, and the clarified and transparent ZrO$_2$ sol was obtained after aging at 25 °C for 12 h.

For the ZrO$_2$ sol, the reactions are as Formulas (1)–(3):

$$Zr(NO_3)_4 + 4H_2O \rightarrow Zr(OH)_4 + 4HNO_3 \tag{1}$$

$$\equiv Zr\text{-}OH + OH\text{-}Zr \equiv \rightarrow Zr\text{-}O\text{-}Zr \equiv + H_2O \tag{2}$$

$$Zr(OH)_4 + 2C_2H_2O_4 \equiv \rightarrow = Zr(C_2O_4)_2 + 4H_2O \tag{3}$$

2.1.2. Preparation of Hydrophilic SiO$_2$ Sol

The molar composition of chemical regents preparing the hydrophilic SiO2 sol was TEOS:MTES:EtOH:H$_2$O:HNO$_3$ = 1.0:0.8:8.0:0.72:0.085. Ethyl orthosilicate (TEOS, p.a. grade, Xi'an chemical reagent Co. Ltd., Xi'an, China) and anhydrous ethanol (EtOH, p.a. grade, Tianjin Branch Micro-Europe Chemical Reagent Co., Ltd., Tianjin, China) were mixed as a hydrophilic solution and placed in an ice water bath. The mixture of H$_2$O and nitric acid (HNO$_3$, p.a. grade, Sichuan Xilong Reagent Co., Ltd., Xilong, China) was added dropwise under a magnetic stirrer for 30 min. After the dropwise addition, the mixture was stirred at reflux for 3 h at 60 °C and cooled to obtain the hydrophilic SiO$_2$ sol.

2.1.3. Preparation of Hydrophobic SiO$_2$ Sol

Methyltriethoxysilane (MTES, grade 98%, Hangzhou Guibao Chemical Co. Ltd., Hangzhou, China) was used as a hydrophobic agent, and according to the molar ratio of TEOS:MTES:EtOH:H$_2$O:HNO$_3$ = 1.0:0.8:8.0:0.72:0.085, it was first mixed completely with MTES, TEOS, and EtOH, placed in an ice-water bath, and stirred fully under a magnetic stirrer for 30 min before adding dropwise H$_2$O and nitric acid mixture, and after the dropwise addition, it was stirred at 60 °C under reflux for 3 h and cooled to obtain methyl-modified hydrophobic SiO$_2$ sol.

2.1.4. Preparation of Hydrophilic and Hydrophobic ZrO$_2$-SiO$_2$ Sols
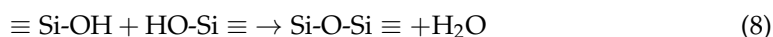
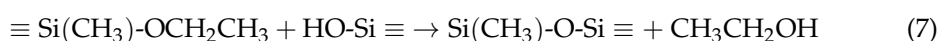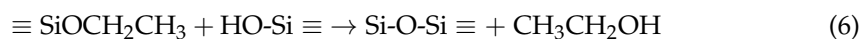According to the Zr/Si molar ratio of 0.15, a mixture of ZrO$_2$ sol was added drop by drop into the freshly prepared SiO$_2$ sols and methyl-modified SiO$_2$, respectively. After stirring strongly for 60 min at 25 °C, the hydrophilic ZrO$_2$-SiO$_2$ and hydrophobic ZrO$_2$-SiO$_2$ sols were obtained, respectively.

The co-hydrolysis and condensation reactions of TEOS and MTES are as Formulas (4)–(9):
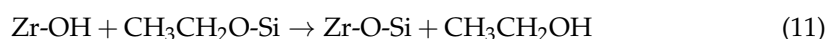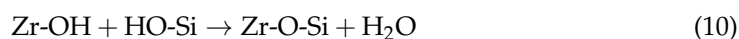
Hydrolysis reactions:

$$Si(OCH_2CH_3)_4 + nH_2O \rightarrow Si(OCH_2CH_3)_{4-n}(OH)_n + nCH_3CH_2OH \quad (4)$$

$$CH_3\text{-}Si(OCH_2CH_3)_3 + nH_2O \rightarrow CH_3\text{-}Si(OCH_2CH_3)_{3-n}(OH)_n + nCH_3CH_2OH \quad (5)$$

Condensation reactions:

$$\equiv SiOCH_2CH_3 + HO\text{-}Si \equiv \rightarrow Si\text{-}O\text{-}Si \equiv + CH_3CH_2OH \quad (6)$$

$$\equiv Si(CH_3)\text{-}OCH_2CH_3 + HO\text{-}Si \equiv \rightarrow Si(CH_3)\text{-}O\text{-}Si \equiv + CH_3CH_2OH \quad (7)$$

$$\equiv Si\text{-}OH + HO\text{-}Si \equiv \rightarrow Si\text{-}O\text{-}Si \equiv + H_2O \quad (8)$$

$$\equiv Si(CH_3)\text{-}OH + HO\text{-}Si \equiv \rightarrow Si(CH_3)\text{-}O\text{-}Si \equiv + H_2O \quad (9)$$

The reactions between ZrO_2 and hydrophilic SiO_2, hydrophobic SiO_2 sols are as Formulas (10) and (11):

$$Zr\text{-}OH + HO\text{-}Si \rightarrow Zr\text{-}O\text{-}Si + H_2O \quad (10)$$

$$Zr\text{-}OH + CH_3CH_2O\text{-}Si \rightarrow Zr\text{-}O\text{-}Si + CH_3CH_2OH \quad (11)$$

2.2. Preparation of Xerogels

The as-prepared ZrO_2, hydrophilic and hydrophobic SiO_2, and hydrophilic and hydrophobic ZrO_2-SiO_2 sols were placed in the Petri dishes, respectively, and dried at 50 °C. The formed gels were ground into powders and then roasted in a program-controlled high-temperature furnace at 400 °C for 2 h under N_2 atmosphere with a heating rate of 1 °C·min^{-1}.

2.3. Characterization

FTIR spectra were recorded on a PerkinElmer Spotlight 400 and Frontier spectrometer and KBr pellets were prepared and taken over a wavelength range of 400–4000 cm^{-1}. XRD patterns were performed on a RigakaD/max 2200 X-ray diffractometer, using CuKα radiation and scanning 2θ from 4 to 90°, operated at 40 kV and 40 mA. The JSM-6700F SEM was used to investigate the morphology of the samples. X-ray photoelectron spectroscopy (XPS) was used to analyze the surface chemical composition of the hydrophilic and hydrophobic ZrO_2-SiO_2 xerogels. (ESCALAB250xi, Thermo Scientific, Waltham, MA, USA). The pressure in the analysis chamber was maintained at 3.0×10^{-7} Pa. The binding energy values were referenced to the C (1 s) line situated at 284.6 eV. N_2 absorption–adsorption isotherms and pore size distributions were obtained from the ASAP2020 Plus automatic analyzer, micromeritics. Molecular structure models were constructed using ChemDraw software 18.0 (PerkinElmer Corporation, Waltham, MA, USA, Software license: Sijie Marking Software Co., Ltd., Suzhou, China).

2.4. Water Adsorption Measurement

To examine the hydrophobicity of the two ZrO_2-SiO_2 xerogels, the hydrophilic and hydrophobic ZrO_2-SiO_2 samples were aged in a constant temperature and humidity chamber of 25 °C and 75% RH. During the aging period, the samples were weighed, and the mass changes and water adsorption were calculated.

2.5. Adsorption Performance Test

The effects of adsorption time, adsorption temperature, dosage, and pH on the removal of RhB were investigated by adsorption experiments. A certain amount of rhodamine B (RhB, Relative molecular weight (Mw) = 479.01, λ_{max} = 552 nm, Tianjin Comio Chemical Reagent Co., Ltd., Tianjin, China) dye was dissolved in deionized water to prepare a

standard solution of 140 mg·L^{-1}. The Zeta potential of the xerogels was measured using a Nano-ZS tester manufactured in the UK and the average of three measurements was taken.

The hydrophilic and hydrophobic ZrO$_2$-SiO$_2$ xerogels (0.01, 0.05, 0.1, 0.15, 0.2 g) were separately dispersed in the above RhB solution (50 mL) under vigorous stirring (700 rpm). The adsorption experiments were conducted at 25, 35, and 45 °C, respectively. The solid–liquid mixture was separated by centrifugation. The liquid phase was analyzed using a UV-V spectrophotometer at a wavelength of 554 nm. The RhB concentrations were then calculated from the calibration curve.

The adsorption amount q_e of RhB by the hydrophilic and hydrophobic ZrO$_2$-SiO$_2$ xerogels ate calculated by Equation (12):

$$q_e = \frac{(C_0 - C_e)V}{W} \tag{12}$$

The removal rate of RhB in water is calculated by Equation (13):

$$R = \frac{C_0 - C_e}{C_0} \times 100\% \tag{13}$$

where C_0 and C_e (mg·L^{-1}) is the initial and equilibrium concentration of RhB, respectively. V (L) is the volume of the solution. W (g) is the dry mass of the xerogels.

2.6. Desorption Performance Test

The hydrophilic and hydrophobic ZrO$_2$-SiO$_2$ xerogels were rinsed with anhydrous ethanol at room temperature, and the process was repeated 6 times for multiple cycles of adsorption and desorption to test the reproducibility of the prepared xerogel adsorbents.

3. Results and Discussion

3.1. FTIR Analysis

The functional groups of ZrO$_2$, hydrophilic and hydrophobic SiO$_2$, and hydrophilic and hydrophobic ZrO$_2$-SiO$_2$ xerogels were investigated using FTIR spectra, shown in Figure 2. In Figure 2, the absorption peak at around 3449 cm^{-1} is the stretching and bending vibration of the -OH group caused by the absorption of water, the characteristic peak at 1634 cm^{-1} is caused by the Si-OH bonds [26] of the xerogel, the peaks located around 790 cm^{-1} are related to the stretching vibration of the Si-O bond [27], and these sets of absorption peaks co-occur in the hydrophilic and hydrophobic SiO$_2$, hydrophilic and hydrophobic ZrO$_2$-SiO$_2$ xerogels. As can be seen in Figure 2, the absorption peak of Si-O-Si in hydrophilic and hydrophobic SiO$_2$ xerogels is 1050 cm^{-1} [28]. In hydrophilic and hydrophobic ZrO$_2$-SiO$_2$ xerogels, the absorption peaks of Zr-O-Si appeared at 1100 cm^{-1}, and the absorption peak at 1110 cm^{-1} is due to the presence of Zr perturbing the three-dimensional asymmetric stretching vibrations of Si-O-Si forming a Zr-O-Si bond, indicating the chemical bonding of SiO$_2$ to ZrO$_2$ particles [29]. The methyl hydrophobic modification of the xerogel is achieved by depleting the -OH group in the Si-OH bond on the xerogel surface and introducing the hydrophobic group -CH$_3$ to form the Si-CH$_3$ bond. Compared with SiO$_2$ and hydrophilic ZrO$_2$-SiO$_2$, the hydrophobic SiO$_2$ and ZrO$_2$-SiO$_2$ exhibited -CH$_3$ absorption peak at 2971 cm^{-1} and Si-CH$_3$ absorption peak at 1277 cm^{-1}, indicating the successful modification of the methyl hydrophobic groups. The characteristic peaks of -OH and Zr-OH can be seen in ZrO$_2$ xerogel at 3400 cm^{-1} and 1410 cm^{-1}, respectively, along with an absorption peak of Zr-O at 447 cm^{-1}. In addition, it can be seen from Figure 2 that the absorption peaks at 3449 cm^{-1} and 1634 cm^{-1} of hydrophobic xerogel are slightly weaker than hydrophilic xerogel, whereas the presence of this indicates the consumption of -OH and the formation of Si-CH$_3$. According to infrared spectrum analysis, combined with the reaction equations, there are Si-O-Si, Zr-O-Si, Si-OH, Zr-OH, and Zr-O groups on the surfaces of hydrophilic and hydrophobic ZrO$_2$-SiO$_2$ xerogels. In addition, the surface of the hydrophobic ZrO$_2$-SiO$_2$ sample also contains Si-CH$_3$ groups.

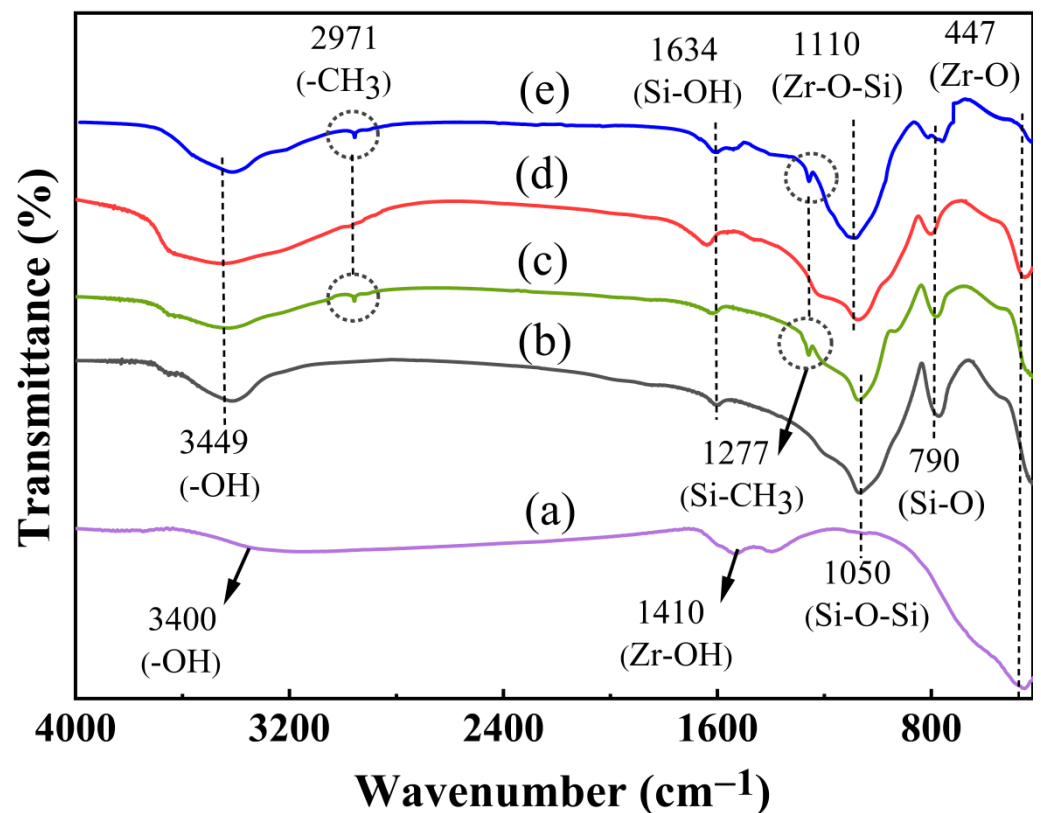**Figure 2.** FTIR spectra comparison of (a) ZrO_2, (b) hydrophilic SiO_2, (c) hydrophobic SiO_2, (d) hydrophilic ZrO_2-SiO_2, and (e) hydrophobic ZrO_2-SiO_2 xerogels.

3.2. Phase Structure Analysis

Figure 3 shows the XRD patterns of ZrO_2, hydrophilic and hydrophobic SiO_2, and hydrophilic and hydrophobic ZrO_2-SiO_2 xerogels. The tetragonal phase ZrO_2 diffraction peaks at $2\theta = 30.57$, 35.26, 50.41, and $60.63°$ can be seen in ZrO_2. In the hydrophilic and hydrophobic SiO_2, and hydrophilic and hydrophobic ZrO_2-SiO_2 xerogels, the distinctive diffraction peaks all appear between $2\theta = 20\sim30°$, related to the presence of amorphous SiO_2. In contrast, the silicon diffraction peak of the hydrophilic and hydrophobic SiO_2 xerogels appears at $2\theta = 20.88°$, whereas the silicon diffraction peaks of the hydrophilic and hydrophobic ZrO_2-SiO_2 xerogels appear at $2\theta = 24.08°$, mainly because the introduced zirconium atoms replaced some silicon atoms and formed the Zr-O-Si bonds, which lead to a decrease in SiO_2 content, the crystal diffraction peaks move to a larger angle. In hydrophilic and hydrophobic ZrO_2-SiO_2 xerogels, because of the formation of Zr-O-Si bonds, the tetragonal t-ZrO_2 crystallographic surfaces appear in the diffraction peaks at $2\theta = 30.57°$, $50.41°$, and $60.63°$ [30]. However, the intensity of the diffraction peak is weak and the dispersion broadens, indicating that the nuclei of t-ZrO_2 are produced with relatively low crystallinity [31]. Comparing before and after the modification, the structures of the xerogels phases were similar and the diffraction peaks did not differ significantly.

The surface chemical composition of the hydrophilic and hydrophobic ZrO_2-SiO_2 xerogels was analyzed by XPS as shown in Figure 4. Figure 4a shows that the Si 2p spectra of the hydrophilic ZrO_2-SiO_2 sample consist of the main component with a binding energy of 103.69 eV due to the Si-O species on the sample surface. The Si 2p spectra of the hydrophobic ZrO_2-SiO_2 sample contain two peaks as shown in Figure 4b. It is reasonable to assign the peak lying at the binding energy of about 103.72 eV mainly to the Si-O species, and the peak lying at the binding energy of around 101.79 eV to the Si-CH_3. It is seen that the chemical environment of the Si on the two sample surfaces changes significantly with the addition of MTES during the sol preparation. Compared with the hydrophilic

sample, the morphology of the Si 2p peak of hydrophobic ZrO_2-SiO_2 xerogel changed significantly, and the Si 2p spectral peak became wider and moved to the direction of low bond energy, which indicated that the chemical bond structure of Si 2p changed significantly after hydrophobic modification by methyl and the bond energy of Si decreased.
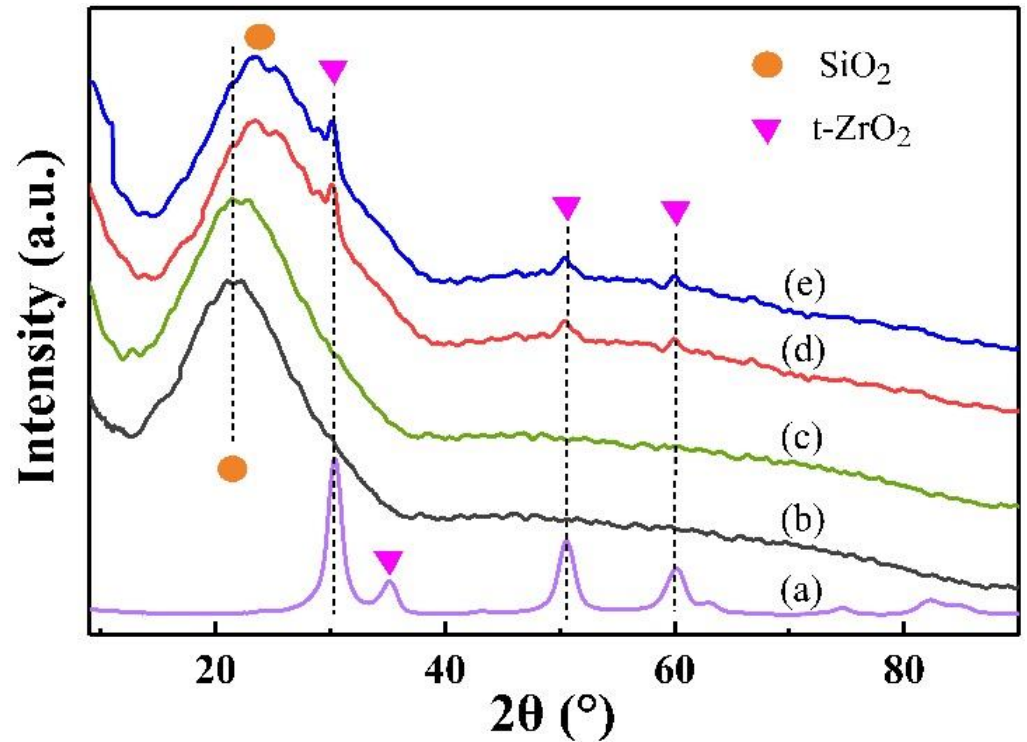

Figure 3. XRD pattern of (a) ZrO_2, (b) hydrophilic SiO_2, (c) hydrophobic SiO_2, (d) hydrophilic ZrO_2-SiO_2, and (e) hydrophobic ZrO_2-SiO_2 xerogels.
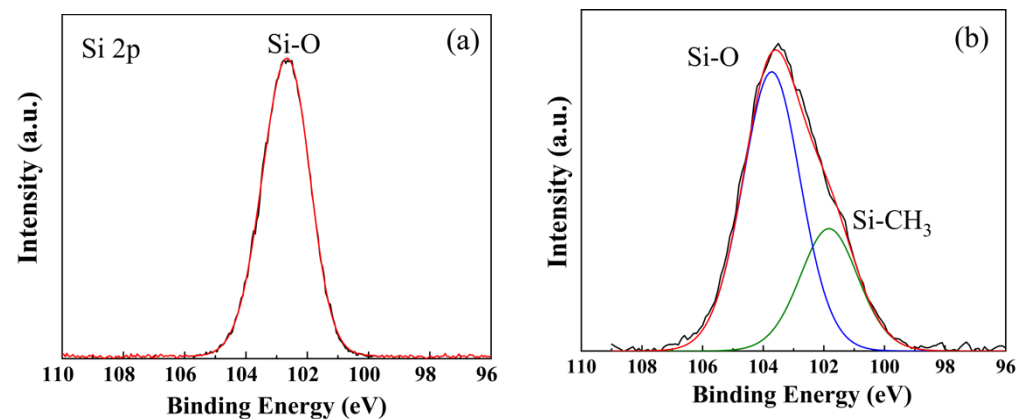

Figure 4. Si 2p spectra of XPS analysis for the (**a**) hydrophilic and (**b**) hydrophobic ZrO_2-SiO_2 xerogels.

3.3. Pore Structure Analysis

Figure 5 shows the molecular structure of ZrO_2, SiO_2, hydrophobic SiO_2, hydrophilic ZrO_2-SiO_2, and hydrophobic ZrO_2-SiO_2. Figure 6 shows the N_2 adsorption–desorption curves of hydrophilic and hydrophobic ZrO_2-SiO_2 xerogels. From Figure 6, the isotherms of hydrophilic and hydrophobic ZrO_2-SiO_2 xerogels showed the type IV isotherms of Brunauer–Deming–Deming–Teller (BDDT) classification, which exhibited a microporous structure at $P/P_0 < 0.4$ and a hysteresis loop near $P/P_0 = 0.4$, indicating the presence of mesopores in the xerogels. It can be seen from Figure 6 that the N_2 adsorption of hydrophobic ZrO_2-SiO_2 xerogel is greater than that of hydrophilic ZrO_2-SiO_2. Compared

with hydrophilic ZrO_2-SiO_2, the N_2 adsorption of hydrophobic ZrO_2-SiO_2 xerogel increased by 30.96%. Figure 7 shows the pore size distributions of the hydrophilic and hydrophobic ZrO_2-SiO_2 xerogels. In Figure 7, it can be seen that the pore size distribution of hydrophilic and hydrophobic ZrO_2-SiO_2 xerogels are similar, and the pore distribution ranges from the micropore to the mesoporous region. In the graph, the total pore volume, specific surface area, and pore size of the hydrophobic ZrO_2-SiO_2 xerogel are greater than those of the hydrophilic ZrO_2-SiO_2 xerogel, mainly because the bond lengths of Si-CH_3 groups in the hydrophobic ZrO_2-SiO_2 xerogel are longer than those of Si-OH in hydrophilic ZrO_2-SiO_2 xerogel (Figure 5), the bond lengths of Si-C (1.88 Å) and C-H (1.1 Å) are longer than those of Si-O (1.65 Å) and O-H (1.01 Å), respectively.
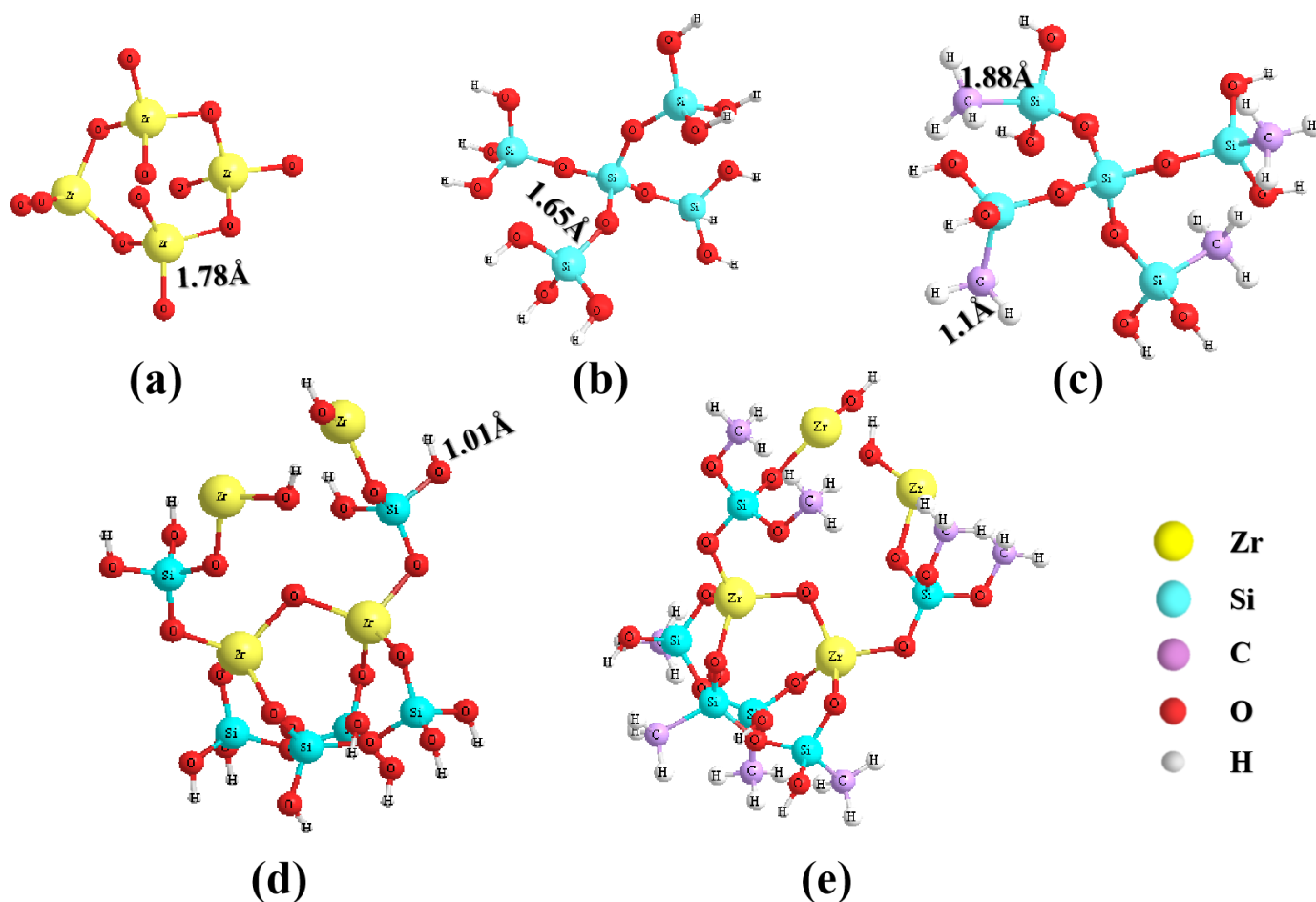

Figure 5. Molecular structural models of (**a**) ZrO_2, (**b**) hydrophilic SiO_2, (**c**) hydrophobic SiO_2, (**d**) hydrophilic ZrO_2-SiO_2, and (**e**) hydrophobic ZrO_2-SiO_2 xerogels.

The pore structure parameters of hydrophilic and hydrophobic ZrO_2-SiO_2 xerogels are shown in Table 1. The average pore size, BET surface area, and total pore volume of hydrophobic ZrO_2-SiO_2 xerogel are larger than those of hydrophilic ZrO_2-SiO_2 xerogel. Compared with the hydrophilic ZrO_2-SiO_2 xerogel, the specific surface area and pore capacity of the hydrophobic ZrO_2-SiO_2 xerogel sample increased by 62.76% and 59.26%, respectively. Generally speaking, the adsorption performance of an adsorbent depends mainly on its surface properties and the BET surface area, whereas a larger BET surface area and a suitable pore size are more favorable [27] for the adsorption of dye molecules. The hydrophobic xerogel was more advantageous.
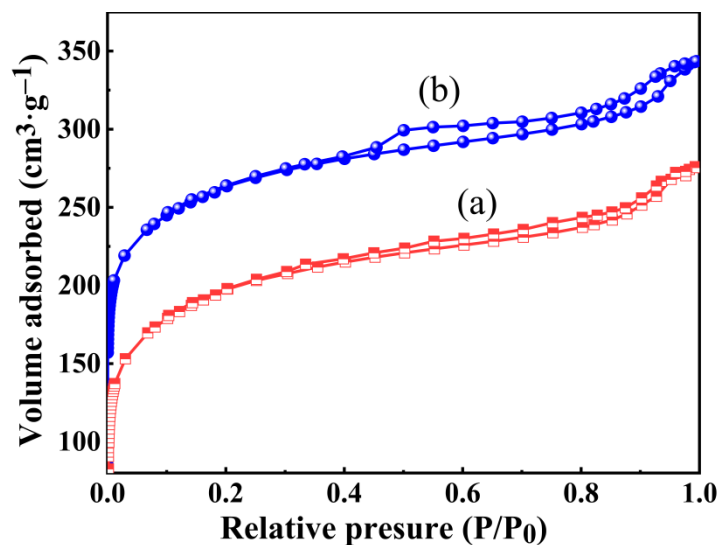
Figure 6. The N_2 adsorption-desorption isotherms for the (a) hydrophilic and (b) hydrophobic ZrO_2-SiO_2 xerogels.
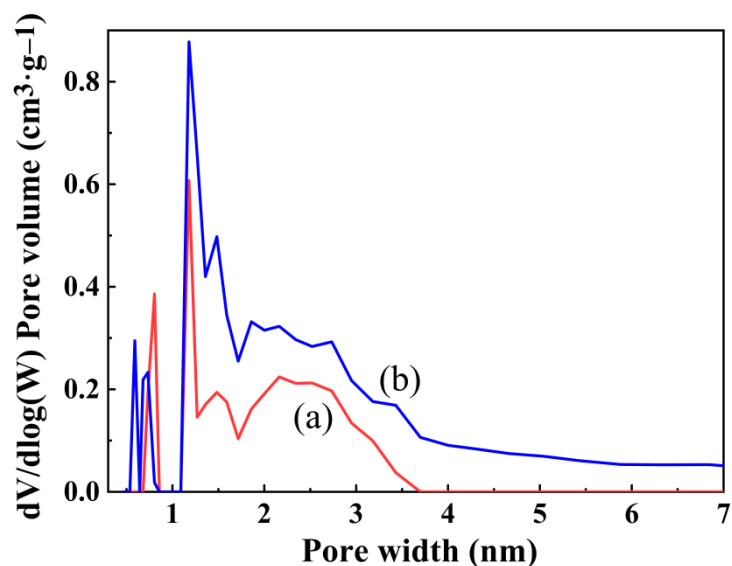

Figure 7. The corresponding pore size distribution curves for the (a) hydrophilic and (b) hydrophobic ZrO_2-SiO_2 xerogels.

Table 1. Pore structure parameters of the hydrophilic and hydrophobic ZrO_2-SiO_2 xerogels.

Samples	BET Surface Area ($m^2 \cdot g^{-1}$)	Average Pore Size (nm)	V_{total} (STP) ($cm^3 \cdot g^{-1}$)
hydrophilic ZrO_2-SiO_2	310.13	2.16	0.27
hydrophobic ZrO_2-SiO_2	504.78	2.35	0.43

3.4. SEM Analysis

The SEM images of hydrophilic and hydrophobic ZrO_2-SiO_2 xerogels are shown in Figure 8. In Figure 8, it can obviously be seen that the particle size of hydrophobic ZrO_2-SiO_2 xerogel is larger than that of the hydrophilic sample. As described in the pore structure analysis, this is a result of the introduction of Si-CH_3 groups, in which the bond lengths of Si-C and C-H are longer than those of Si-O and O-H, respectively.
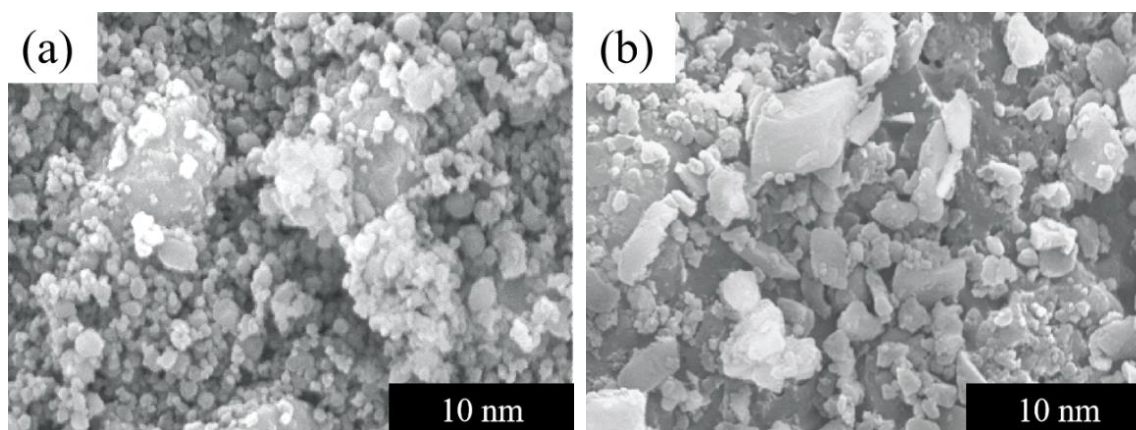
Figure 8. SEM comparison of (**a**) hydrophilic ZrO_2-SiO_2, (**b**) hydrophobic ZrO_2-SiO_2 xerogels.

3.5. Water Absorption Analysis

　　The water absorption of hydrophilic and hydrophobic ZrO_2-SiO_2 xerogels was an-alyzed, shown in Figure 9. As shown in Figure 9, with the increase in aging time, the water absorption of the two ZrO_2-SiO_2 samples gradually increased. It reached its satu-rated state after 6 d, and the saturated water absorption was about 10.55% and 5.33% for the hydrophilic and hydrophobic samples, respectively. Compared with the hydrophilic ZrO_2-SiO_2 xerogel, the water absorption of the hydrophobic sample decreased by 49.5%. The water absorption of porous materials is related to their hydrophobicity and specific surface area. In general, more hydrophilic surfaces and larger specific surface areas cor-respond to greater water absorption. As shown in Table 1, the specific surface area of the hydrophobic ZrO_2-SiO_2 xerogel is larger than that of the hydrophilic one. This means that the introduced Si-CH_3 bonds in the hydrophobic ZrO_2-SiO_2 xerogel have higher hydrophobicity than the Si-OH bonds, which can lead to less water absorption.
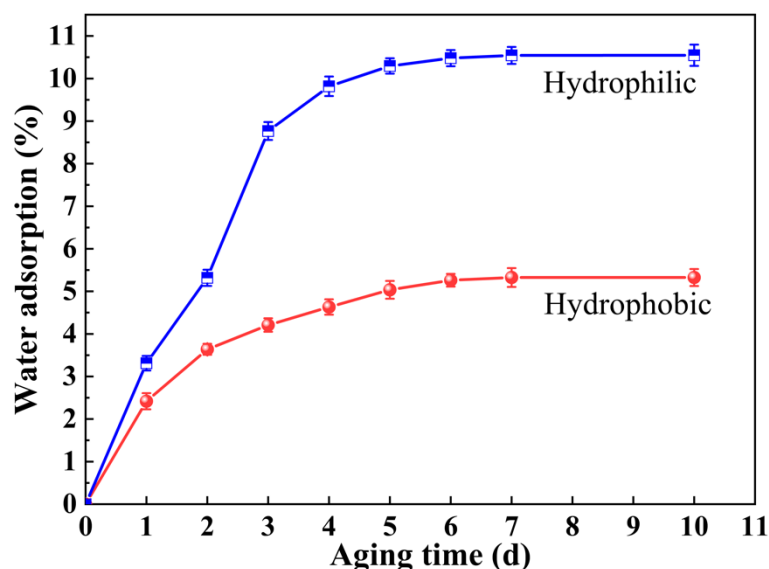
Figure 9. Water absorption diagram of hydrophilic ZrO_2-SiO_2 and hydrophobic ZrO_2-SiO_2 xerogels.

3.6. Adsorption Performance Studies

3.6.1. Effect of Adsorption Time and Temperature

　　Figure 10 shows the effect of the adsorption capacity of hydrophilic and hydrophobic ZrO_2-SiO_2 xerogel with the change in adsorption time and adsorption temperature. As shown in Figure 10, the hydrophobic xerogel exhibited rapid adsorption during the first

30 min, after which it was basically in adsorption equilibrium. The hydrophilic xerogel was basically in adsorption equilibrium at 120 min. The adsorption amounts of hydrophilic and hydrophobic xerogels increased by 10.88 mg·g^{-1} and 15.18 mg·g^{-1} with increasing temperature, respectively, and reached the maximum adsorption amount at 45 °C. In addition, the adsorption capacity of the hydrophobic xerogel was increased by 70.3% relative to that of hydrophilic ZrO_2-SiO_2 xerogel. The results showed that the hydrophobic xerogel had a superior adsorption effect on the RhB solution. As seen in Figure 10, the adsorption process of hydrophobic ZrO_2-SiO_2 on RhB was endothermic, and in general, the normal adsorption process is exothermic. However, if the adsorption process is influenced by intraparticle diffusion, the adsorption capacity will increase with temperature due to the heat absorption of the diffusion process [27]. This means that increasing the temperature increases the diffusion rate of adsorbent RhB molecules between the outer boundary layer and the inner pores of the hydrophobic ZrO_2-SiO_2 xerogel, thus increasing the adsorption capacity of hydrophobic ZrO_2-SiO_2.

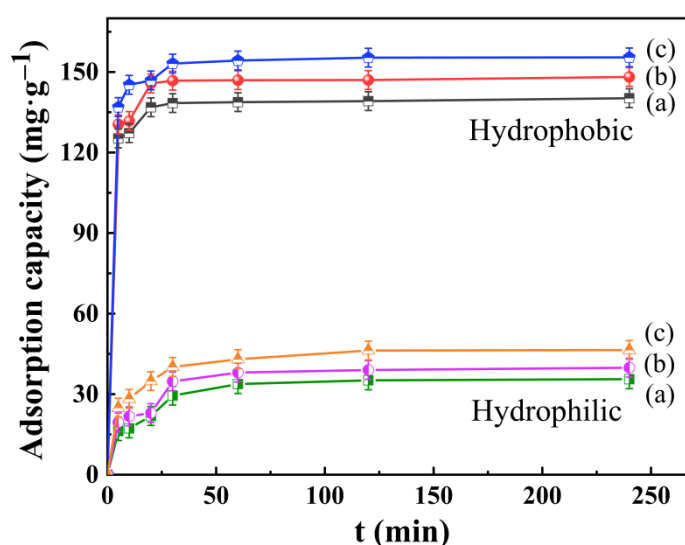**Figure 10.** Effect of hydrophilic and hydrophobic ZrO_2-SiO_2 xerogels at various adsorption temperatures (a) 25 °C, (b) 35 °C, and (c) 45 °C on the adsorption capacity of RhB (pH = 7, RhB concentration = 140 mg·L^{-1}).

As the hydrophobic ZrO_2-SiO_2 xerogel contains methyl groups on its surface, the RhB surface is also rich in methyl groups (Figure 1), making the hydrophobic xerogel similarly soluble with RhB and providing a better adsorption effect. Therefore, the hydrophobic ZrO_2-SiO_2 xerogel was chosen for the subsequent experiments.

3.6.2. Effect of Dosage

Figure 11 shows the adsorption capacity for the unit mass of RhB by hydrophilic and hydrophobic ZrO_2-SiO_2 xerogels with various dosages. It can be seen from Figure 11 that the removal rate of both samples increased with the increase in the dosage, whereas the maximum removal rate of the hydrophobic xerogel was 23.03% higher than that of the hydrophilic one. In addition, the adsorption capacity for the unit mass of both xerogels reached the maximum value at the dosage of 0.01 g and decreased gradually with the increase in dosage. When the dose was increased from 0.01 g to 0.05 g, the adsorption per unit mass decreased by 7.6 mg·g^{-1} and 8.3 mg·g^{-1} for hydrophilic and hydrophobic xerogels, respectively. The total amount of adsorption increased with increasing dose, whereas the adsorption per unit mass decreased gradually. The reason is that as the amount of RhB remains unchanged, with the gradual increase in the amount of adsorbent, the number of adsorption active sites in the system increases and the adsorption rate accelerates, which leads to a decrease in the utilization of adsorption active sites per unit

mass of adsorbent, resulting in a lower adsorption amount for unit mass. The adsorption capacity for the unit mass of hydrophobic ZrO_2-SiO_2 xerogel was higher than those of hydrophilic ZrO_2-SiO_2 xerogel because the introduced -CH_3 group increased the specific surface area and the contact area with RhB solution, and the adsorption capacity of the hydrophobic xerogel increased by 66.1% and 71.5% relative to the hydrophilic at 0.01 g and 0.05 g, respectively. Therefore, the highest utilization rate was achieved at the dosage of 0.05 g.
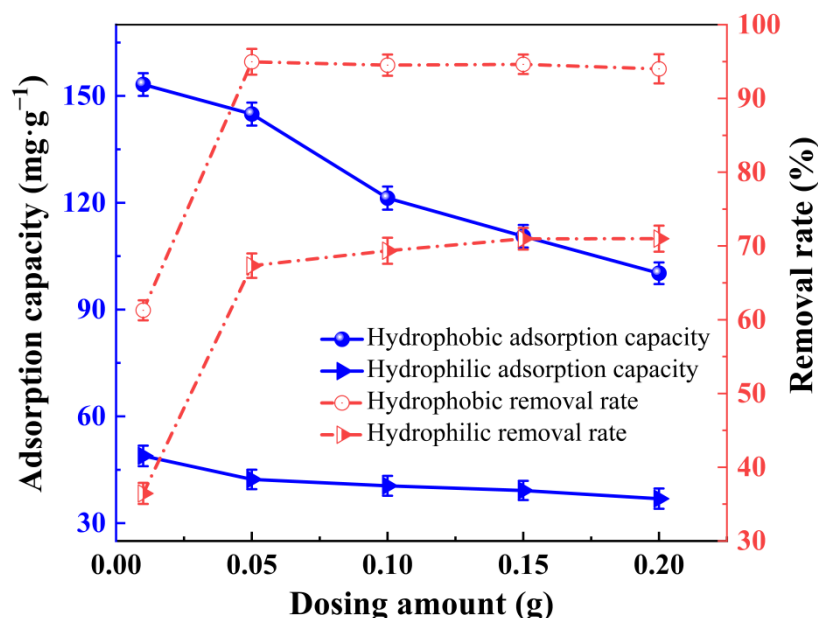

Figure 11. Effect of hydrophilic and hydrophobic ZrO_2-SiO_2 xerogels on the adsorption capacity and removal rate for unit mass of RhB at various dosages (pH = 7, contact time = 120 min, RhB concentration = 140 mg·L^{-1}; T = 25 °C).

3.6.3. Effect of pH

In the adsorption experiments, the solution pH is an important factor in controlling the adsorption process and may have a great influence on the final adsorption effect, because it affects the surface charge of the adsorbent in the solution as well as the degree of ionization and molecular structure of the dyes [27]. The adsorption capacities of RhB for the hydrophilic and hydrophobic ZrO_2-SiO_2 xerogels at different pH were shown in Figure 12. In Figure 12, the variation of adsorption capacity for the two samples showed similar trends. With the increases in pH value, the adsorption capacities of RhB for the hydrophilic and hydrophobic ZrO_2-SiO_2 xerogels tended to decrease gradually, which had a maximum of 52.42 and 169.23 mg·g^{-1} at pH = 3, respectively. When the pH value increased from 3 to 11, the adsorption capacities of RhB for the hydrophilic and hydrophobic samples decreased by 55.5% and 31.0%, respectively. The effect of solution pH on the zeta potentials of the two adsorbents is shown in Figure 13. At pH = 3–11, the two adsorbents both had a negative zeta potential and their absolute values increased with the increasing pH value. Furthermore, the absolute value of the zeta potential of the hydrophilic sample was greater than that of the hydrophobic one at the same pH value. RhB is a cationic basic dye and its acid dissociation constant pKa is at about 3.2. When pH = 3, the RhB is presented in cationic and monomeric molecular form, there is electrostatic attraction existing between RhB and the two adsorbents. Thus, the organic skeleton of RhB easily can enter into the pores of the xerogels. When pH = 5–11, the RhB exists in the form of zwitterions. At the time, they are not easy to enter into the pore structure. In the process of adsorption of RhB by the adsorbents, the electrostatic mechanism is not only the mechanism of dye adsorption in this system but also the interaction between the adsorbents and dye molecules via hydrogen bonds and hydrophobic structures. The hydrophobic ZrO_2-SiO_2

xerogel has the hydrophobic Si-CH$_3$ groups, whereas the hydrophilic sample does not. This further increases the adsorption capacity of hydrophobic xerogel to RhB. Furthermore, the results indicate that the acidic environment is favorable for the adsorption of RhB by the hydrophilic and hydrophobic ZrO$_2$-SiO$_2$ xerogels.
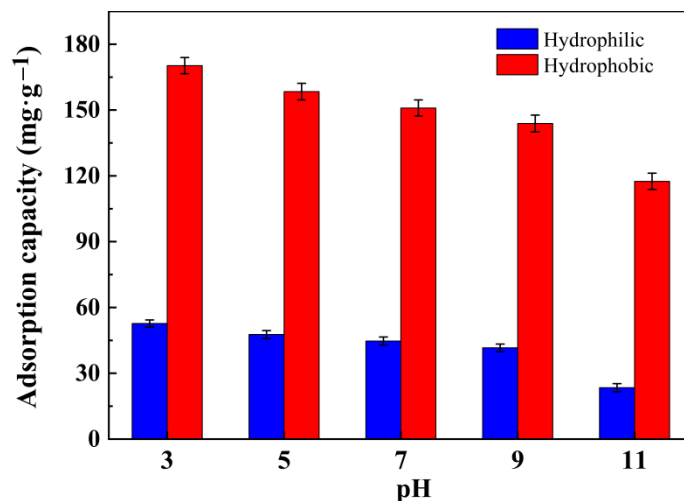
Figure 12. Adsorption capacities of RhB for the hydrophilic and hydrophobic ZrO$_2$-SiO$_2$ xerogels at different pH (dosage = 0.05 g, contact time = 120 min, RhB concentration = 140 mg·L^{-1}, T = 25 °C).
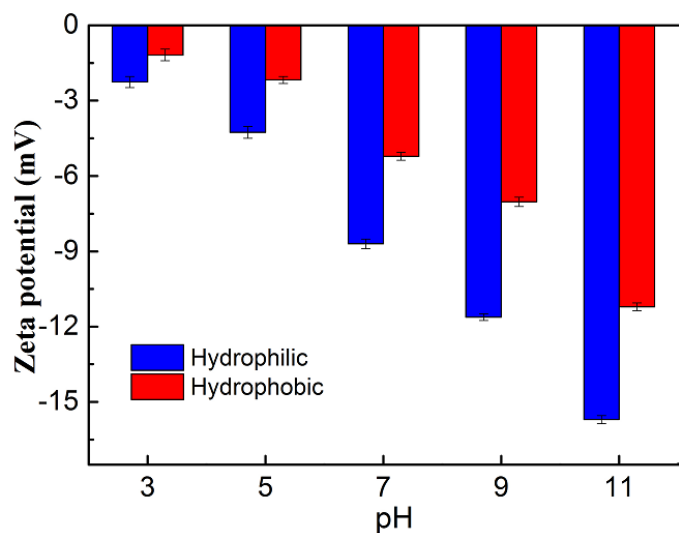
Figure 13. Effect of solution pH on the zeta potentials of hydrophilic and hydrophobic ZrO$_2$-SiO$_2$ xerogels.

3.7. Adsorption Kinetic Analysis

The adsorption kinetic analysis process is designed to investigate the kinetics and mechanism of adsorption of RhB by hydrophobic ZrO$_2$-SiO$_2$ xerogel, and it includes pseudo–first-order dynamics, pseudo–second-order dynamics, and intra-particle diffusion models. The experimental data were fitted by a kinetic sorption model [32,33], which was calculated and fitted using Equations (14) and (15). The fitting results are shown in Table 2 and Figure 14a–c.

Table 2. Adsorption kinetic parameters of RhB on hydrophobic ZrO_2-SiO_2 xerogel at various temperatures.

Kinetic Model	Kinetic Parameters	Temperature (K)		
		298.15	308.15	318.15
q_e		169.23	170.05	178.98
Pseudo–first-order	K_1	0.0068	0.0058	0.0075
	R^2	0.9112	0.9886	0.9768
Pseudo–second-order	K_2	0.0083	0.0063	0.0071
	R^2	0.9805	0.9832	0.9961
intra-particle diffusion	K_{di}	2.1038	2.9532	3.8449
	R^2	0.9015	0.9594	0.9483
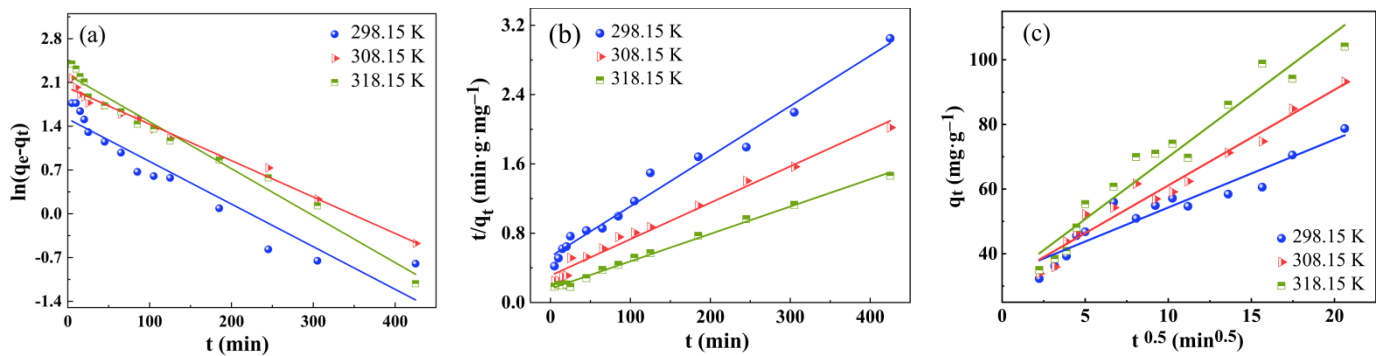
Figure 14. Adsorption kinetics of RhB adsorbed by hydrophobic ZrO_2-SiO_2 xerogel: (**a**) pseudo–first-order kinetic plots, (**b**) pseudo–second-order kinetic plots, and (**c**) intra-particle diffusion plots (dosage = 0.05 g, pH = 3, RhB concentration = 140 mg·L^{-1}, contact time = 120 min, T = 298.15, 308.15, and 318.15 K).

The calculation of the pseudo–first-order dynamics is given in equation:

$$\ln(q_e - q_t) = \ln q_e - K_1 t \tag{14}$$

The calculation of the pseudo–second-order dynamics is given in equation:

$$\frac{t}{q_t} = \frac{1}{K_2 q_e^2} + \frac{t}{q_e} \tag{15}$$

The adsorption rate is usually controlled by membrane diffusion, intra-particle diffusion, or both of them. The first–second-order and pseudo–second-order kinetic models cannot determine the role of intra-particle diffusion in the adsorption dynamics process. In order to identify whether the intra-particle diffusion is a rate-limiting step in the adsorption kinetics process or not, the experimental data is further fitted by the intra-particle diffusion model [34], and the calculation formula is shown in (16):

$$q_t = K_{di} t^{0.5} + C \tag{16}$$

where t (min) is the adsorption time. q_e and q_t (mg·g^{-1}) are the adsorption capacities at equilibrium and at time t, respectively. K_1 (min^{-1}) and K_2 (g·mg^{-1}·min^{-1}) are the pseudo–first-order and pseudo–second-order adsorption rate constants (min^{-1}), respectively. K_{di} (mg·g^{-1}·min$^{-0.5}$) is the intra-particle diffusion rate constant. C represents the greater effect of the boundary layer on molecule diffusion.

The high values of R^2 in Table 2 indicate that the adsorption of RhB onto hydrophobic ZrO_2-SiO_2 xerogel can be approximated more appropriately by a pseudo–second-order kinetic model. According to the pseudo–second-order model, the boundary layer resistance is not a rate-limiting step [35]. Moreover, the investigation of diffusion mechanism

with the intra-particle diffusion model is important. The linear fitting result is shown in Figure 14c. The linearity is attributed to the mesopores diffusion, which is an accessible site of adsorption. The fitted lines did not pass through the origin; hence, the adsorption rate is affected by both intra-particle diffusion and film diffusion. In short, the adsorption of RhB onto hydrophobic ZrO$_2$-SiO$_2$ xerogel is a complex process. The related plots in Figure 14a–c indicate that the RhB adsorption reaction proceeds through three steps: the first stage is the rapid adsorption phase of the outer surface (film diffusion), the second stage is the slow adsorption stage (pore or intra-particle diffusion), and the third stage is the adsorption equilibrium stage which means the adsorption reaction is no longer carried out.

3.8. Adsorption Isotherm Analysis

In order to understand the interactions of RhB with the hydrophobic ZrO$_2$-SiO$_2$ xerogel, the Langmuir [36], Freundlich [37] and Dubinin–Radushkevih (D–R) models [38] are used at 298.15, 308.15 and 318.15 K, respectively. To describe the adsorption behavior of RhB onto the hydrophobic ZrO$_2$-SiO$_2$ xerogel as follow:

The calculation of the Langmuir model is given in Equation (17):

$$\frac{1}{q_e} = \frac{1}{q_m b C_e} + \frac{1}{q_m} \tag{17}$$

where b (L·mg^{-1}) is the Langmuir constant. q_m is the maximum monolayer adsorption capacity (mg·g^{-1}), the Langmuir isotherm plots of $1/q_e$ versus $1/C_e$ are given in Figure 15a, and the parameters are exhibited in Table 3.
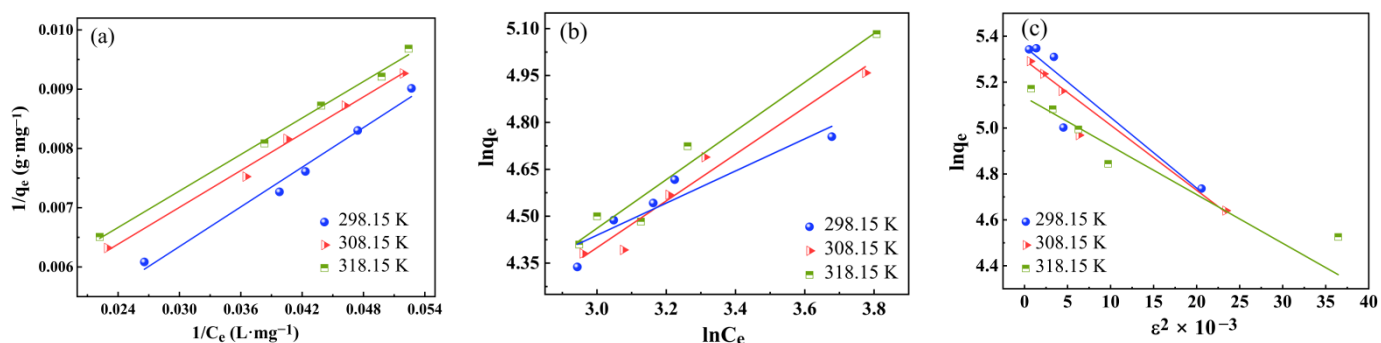
Figure 15. (**a**) Langmuir, (**b**) Freundlich and, (**c**) D–R adsorption isotherm of RhB onto hydrophobic ZrO$_2$-SiO$_2$ xerogel (dosage = 0.05 g, pH = 3, RhB concentration = 140 mg·L^{-1}, contact time = 120 min, T = 298.15, 308.15 and 318.15 K).

Table 3. Adsorption isotherm parameters of RhB on hydrophobic ZrO$_2$-SiO$_2$ xerogel at various temperatures.

Adsorption Isotherm	Isothermal Parameters	Temperature (K)		
		298.15	308.15	318.15
Langmuir	b	0.0031	0.0039	0.0042
	q_m	139.77	154.64	173.53
	R^2	0.9924	0.9939	0.9961
	R_L	0.1231	0.1191	0.1123
Freundlich	K_F	18.1367	8.6576	8.3704
	$1/n$	0.5138	0.7471	0.7789
	R^2	0.8826	0.9647	0.9631
D–R	E	4.0285	4.1893	4.7584
	R^2	0.9302	0.9951	0.8438

Dimensionless constant (R_L) [39] was used to identify the feasibility and favorability of the adsorption process. R_L is calculated in each case using the Equation (18):

$$R_L = \frac{1}{1 + bC_0} \tag{18}$$

The values of R_L reveal that the isotherms are irreversible ($R_L = 0$), unfavorable ($R_L > 1$), favorable ($0 < R_L < 1$), or linear ($R_L = 1$) [40].

The calculation of the Freundlich isotherm model is given in Equation (19):

$$\ln q_e = \ln K_F + \frac{1}{n} \ln C_e \tag{19}$$

where K_F (L·g^{-1}) and n are the Freundlich constant related to adsorption capacity and adsorption intensity, respectively. The Freundlich isotherm plots of $\ln q_e$ versus $\ln C_e$ are shown in Figure 15b and the parameters are exhibited in Table 3.

In order to determine the type of adsorption reaction, the calculation of the Dubinin–Radushkevich (D–R) isotherm model (Figure 15c) is given in Equations (20)–(22):

$$\ln q_e = \ln q_D - B \cdot \varepsilon^2 \tag{20}$$

$$\varepsilon = RT \ln \left(1 + \frac{1}{C_e}\right) \tag{21}$$

$$E = \frac{1}{\sqrt{2B}} \tag{22}$$

where q_D is the theoretical saturation capacity, mg·g^{-1}. B is the adsorption energy constant, mol^2·J^{-2}. ε is the Polanyi potential energy, J·mol^{-1}. R is the ideal gas constant, 8.314 J·mol^{-1}·K^{-1}. T is the thermodynamic temperature, K. E is the average adsorption energy, kJ·mol^{-1}.

From Figure 15 and Table 3, it is seen that the Langmuir isotherm model is more suitable for the RhB adsorption onto hydrophobic ZrO$_2$-SiO$_2$ xerogel with R^2 values greater than 0.99 for both and that the adsorption process may be monolayer adsorption. Maximum adsorption capacity increased with an increase in the temperature from 139.77 mg·g^{-1} to 173.53 mg·g^{-1}, revealing the endothermic nature of the adsorption process. As can be seen in Table 3, for the dimensionless constants, R_L values (0.1123~0.1231) are all less than 1, which indicates that RhB adsorption of hydrophobic ZrO$_2$-SiO$_2$ xerogel is favorable. In addition, the adsorption constant $0 < (1/n) < 1$ of the Freundlich model indicates that the hydrophobic ZrO$_2$-SiO$_2$ xerogel has inhomogeneous surface properties and RhB is easily adsorbed on the surface of the hydrophobic ZrO$_2$-SiO$_2$ xerogel. With the increase in adsorption temperature, the adsorption energy (E) increases. It is indicated that the adsorption of RhB onto hydrophobic ZrO$_2$-SiO$_2$ xerogel is an endothermic behavior. As can be seen from Table 3, the calculated E values are found to be less than 8 kJ·mol^{-1}, indicating that the adsorption process is mainly physical adsorption [41]. The results of this experiment also confirm the better prospect of hydrophobic ZrO$_2$-SiO$_2$ composites for the removal of dye wastewater.

Table 4 shows the comparison of Langmuir parameters for different adsorbents from different researchers. From Table 4, it can be seen that the R^2 of these adsorbent materials is close to 1, which indicates that the adsorption is relatively good. The R_L values are also all less than 1, which indicates that the adsorption is irreversible. The data show that the maximum adsorption capacity of the hydrophilic adsorbent in the fourth cited paper is 177.7 mg·g^{-1}, however, its equilibrium adsorption capacity is only about 120 mg·g^{-1} and the preparation method is different, and the equilibrium adsorption capacity in this paper is as high as 169.23 mg·g^{-1}. This means that the maximum adsorption capacity of the hydrophobic SiO$_2$-ZrO$_2$ xerogel prepared in this paper is higher than the average value of

most adsorbents. Therefore, it indicates that the hydrophobically modified adsorbent in this paper is successful.

Table 4. Langmuir parameters of materials for RhB adsorption from various researchers.

Material Type	R^2	q_m	R_L
Montmorillonite [42]	0.9864	42.19	0.309
Kaolinite [14]	0.98	46.08	0.94
Carbon xerogel [43]	0.9976	147.1	0.058
Hydrophilic ZrO_2-SiO_2 xerogel [24]	0.998	177.7	0.843
Hydrophobic ZrO_2-SiO_2 xerogel (this work)	0.9961	173.53	0.1123

4. Reusability of Xerogel Adsorbent

In addition to the high adsorption capacity, the regeneration and recycling properties of the xerogel are important for a potential application. Figure 16 shows the recycling performance of hydrophobic ZrO_2-SiO_2 xerogel at different recycling times. As shown in Figure 16, the xerogel samples were easily separated from the RhB solution with ethanol. After adsorption, the xerogel was washed with ethanol at room temperature and reused to adsorb RhB again. This regeneration procedure was repeated five times, and the adsorption capacity of the hydrophobic ZrO_2-SiO_2 xerogel decreased from 169.23 mg·g^{-1} to 115.74 mg·g^{-1}, and the adsorption capacity decreased by 31.6%. The results show that the hydrophobic ZrO_2-SiO_2 xerogel has good reusability for the adsorption of RhB and can be used repeatedly many times.
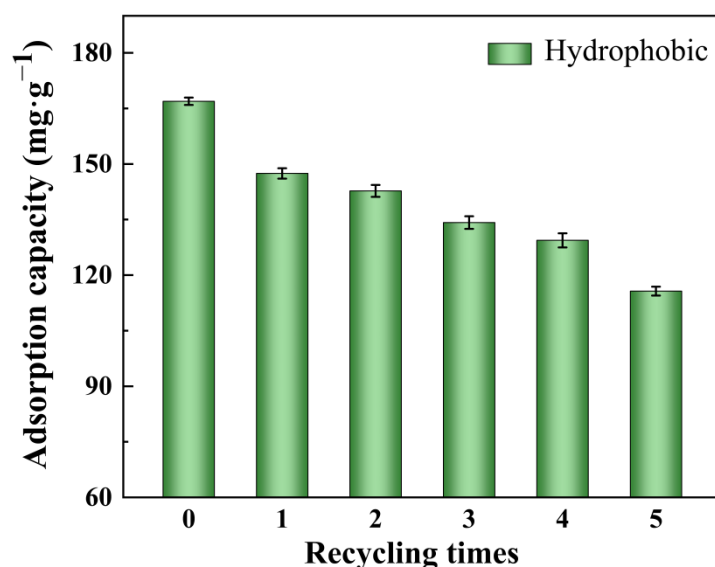

Figure 16. Recycling performance of hydrophobic ZrO_2-SiO_2 xerogel at different recycling times.

5. Conclusions

In this paper, the hydrophilic and hydrophobic ZrO_2-SiO_2 xerogels were prepared by the sol–gel method. The results showed that the hydrophobic Si-CH$_3$ groups were introduced by MTES modification. There are Si-O-Si, Zr-O-Si, Si-OH, Si-CH$_3$, Zr-OH, and Zr-O groups on the surfaces of hydrophobic ZrO_2-SiO_2 xerogel. The hydrophobic ZrO_2-SiO_2 xerogel has a larger specific surface area, mean pore size, and pore volume. A high adsorption capacity of 169.23 mg·g^{-1} for the hydrophobic ZrO_2-SiO_2 xerogel was achieved at 25 °C and pH = 3. The adsorption data fit well with the pseudo–second-order dynamics model and the isothermal adsorption curve fitting showed that the adsorption process of hydrophobic ZrO_2-SiO_2 on RhB was both monolayer adsorption and non-uniform adsorption, and the isothermal adsorption model at different temperatures was consistent with the Langmuir isotherm model. The results from the D–R model indicate

the adsorption of RhB by hydrophobic ZrO_2-SiO_2 xerogel is mainly physical adsorption, accompanied by a spontaneous endothermic process. In future work, we will further investigate the adsorption performance of the hydrophobic ZrO_2-SiO_2 xerogel to other dyes and mixed dyes, comparing the similarities and differences in the adsorption of single-component and multi-component dye molecules.

Author Contributions: Conceptualization, Y.L. and J.Y.; writing—original draft preparation, Y.L. and J.Y.; funding acquisition, J.Y. All authors have read and agreed to the published version of the manuscript.

Institutional Review Board Statement: Not applicable.

Informed Consent Statement: Not applicable.

Data Availability Statement: Not applicable.

Conflicts of Interest: The authors declare no conflict of interest.

References

1. Richardson, S.D.; Willson, C.S.; Rusch, K.A. Use of rhodamine water tracer in the marshland upwelling system. *Groundwater* **2004**, *42*, 678–688. [CrossRef]
2. Li, W.; Mu, B.; Yang, Y. Feasibility of industrial-scale treatment of dye wastewater via bio-adsorption technology. *Bioresour. Technol.* **2019**, *277*, 157–170. [CrossRef]
3. Konstantinou, I.K.; Albanis, T.A. TiO$_2$-assisted photocatalytic degradation of azo dyes in aqueous solution: Kinetic and mechanistic investigations: A review. *Appl. Catal. B Environ.* **2004**, *49*, 1–14. [CrossRef]
4. Amir, M.; Kurtan, U.; Baykal, A. Rapid color degradation of organic dyes by Fe$_3$O$_4$@ His@ Ag recyclable magnetic nanocatalyst. *J. Ind. Eng. Chem.* **2015**, *27*, 347–353. [CrossRef]
5. Robinson, T.; McMullan, G.; Marchant, R.; Nigam, P. Remediation of dyes in textile effluent: A critical review on current treatment technologies with a proposed alternative. *Bioresour. Technol.* **2001**, *77*, 247–255. [CrossRef]
6. Ma, Y.; Yao, J. Photodegradation of Rhodamine B catalyzed by TiO$_2$ thin films. *J. Photochem. Photobiol. A Chem.* **1998**, *116*, 167–170. [CrossRef]
7. Othman, N.H.; Alias, N.H.; Shahruddin, M.Z.; Abu Bakar, N.F.; Him, N.R.N.; Lau, W.J. Adsorption kinetics of methylene blue dyes onto magnetic graphene oxide. *J. Environ. Chem. Eng.* **2018**, *6*, 2803–2811. [CrossRef]
8. Hasanzadeh, M.; Simchi, A.; Far, H.S. Nanoporous composites of activated carbon-metal organic frameworks for organic dye adsorption: Synthesis, adsorption mechanism and kinetics studies. *J. Ind. Eng. Chem.* **2020**, *81*, 405–414. [CrossRef]
9. Brillas, E.; Martínez-Huitle, C.A. Decontamination of wastewaters containing synthetic organic dyes by electrochemical methods. *Appl. Catal. B Environ.* **2015**, *166*, 603–643. [CrossRef]
10. Molla, A.; Li, Y.; Mandal, B.; Kang, S.G.; Hur, S.H.; Chung, J.S. Selective adsorption of organic dyes on graphene oxide: Theoretical and experimental analysis. *Appl. Surf. Sci.* **2019**, *464*, 170–177. [CrossRef]
11. Xaba, M.S.; Noh, J.H.; Mokgadi, K.; Meijboom, R. Kinetic and catalytic analysis of mesoporous metal oxides on the oxidation of Rhodamine B. *Appl. Surf. Sci.* **2018**, *440*, 1130–1142. [CrossRef]
12. Chen, J.; Zhu, X. Magnetic solid phase extraction using ionic liquid-coated core-shell magnetic nanoparticles followed by high-performance liquid chromatography for determination of Rhodamine B in food materials. *Food Chem.* **2016**, *200*, 10–15. [CrossRef]
13. Kyzas, G.Z. A Decolorization Technique with Spent "Greek Coffee" Grounds as Zero-Cost Adsorbents for Industrial Textile. *Wastewaters Mater.* **2012**, *5*, 2069–2087.
14. Khan, T.A.; Dahiya, S.; Ali, I. Use of kaolinite as adsorbent: Equilibrium, dynamics and thermodynamic studies on the ad-sorption of Rhodamine B from aqueous solution. *Appl. Clay Sci.* **2012**, *69*, 58–66. [CrossRef]
15. Gole, J.L.; Prokes, S.M.; Stout, J.D.; Glembocki, O.J.; Yang, R. Unique Properties of Selectively Formed Zirconia Nanostructures. *Adv. Mater.* **2006**, *18*, 664–667. [CrossRef]
16. Liu, H.; Sha, W.; Cooper, A.T.; Fan, M. Preparation and characterization of a novel silica aerogel as adsorbent for toxic organic compounds. *Colloids Surf. A Physicochem. Eng. Asp.* **2009**, *347*, 38–44. [CrossRef]
17. Liu, H.; Li, M.; Liu, J.; Xu, Y.; Qian, G. Phosphate adsorption on metal oxides and metal hydroxides: A comparative review. *Environ. Rev.* **2016**, *24*, 319–332. [CrossRef]
18. Ali, A.A.; Shama, S.A.; Amin, A.S.; EL-Sayed, S.R. Synthesis and characterization of ZrO_2/CeO_2 nanocomposites for efficient removal of Acid Green 1 dye from aqueous solution. *Mater. Sci. Eng. B* **2021**, *269*, 115167. [CrossRef]
19. Lin, Y.F.; Liang, F.L. ZrO_2/carbon aerogel composites: A study on the effect of the crystal ZrO_2 structure on cationic dye adsorption. *Taiwan. Inst Chem.* **2016**, *65*, 78–82. [CrossRef]

20. Shishmakov, A.B.; Mikushina, Y.V.; Petrov, L.A. Synthesis of TiO_2 and TiO_2-SiO_2 xerogels by hydrolysis of tetrabutoxytitanium and tetraethoxysilane in acetic acid atmosphere. *Russ. Chem. Bull.* **2018**, *67*, 1530–1533. [CrossRef]

21. Yang, J.; Wang, X.; Zhao, Y.; Mu, R.; Li, B.; Hou, H. Performance analysis and comparison of methyl-modified Al_2O_3/SiO_2 xerogels fabricated by two methods. *Int. J. Mater. Res.* **2021**, *112*, 17–24. [CrossRef]

22. Shishmakov, A.B.; Molochnikov, L.S.; Antonov, D.O.; Mikushina, Y.V.; Koryakova, O.V.; Petrov, L.A. Synthesis of ZrO_2-SiO_2 and ZrO_2-SiO_2-Cu (II) xerogels by joint hydrolysis in an aqueous ammonia atmosphere. *Russ. Inorganic. Chem.* **2016**, *61*, 1085–1091.

23. Viter, V.N. Sol-gel synthesis of mesoporous mixed oxides in the ZrO_2-SiO_2 system. *Russ. J. Appl. Chem.* **2010**, *83*, 195–199. [CrossRef]

24. Huang, G.; Li, W.; Song, Y. Preparation of SiO_2-ZrO_2 xerogel and its application for the removal of organic dye. *J. Sol-Gel Sci. Technol.* **2018**, *86*, 175–186. [CrossRef]

25. Santos, M.A.F.; Lôbo, I.P.; Cruz, R.S. Synthesis and characterization of novel ZrO_2-SiO_2 mixed oxides. *Mater. Res.* **2014**, *17*, 700–707. [CrossRef]

26. Catauro, M.; Barrino, F.; Dal Poggetto, G.; Milazzo, M.; Blanco, I.; Ciprioti, S.V. Structure, drug absorption, bioactive and antibacterial properties of sol-gel SiO_2/ZrO_2 materials. *Ceram. Int.* **2020**, *46*, 29459–29465. [CrossRef]

27. Aljerf, L. High-efficiency extraction of bromocresol purple dye and heavy metals as chromium from industrial effluent by adsorption onto a modified surface of zeolite: Kinetics and equilibrium study. *J. Environ. Manag.* **2018**, *225*, 120–132. [CrossRef]

28. Cireli, A.; Onar, N.; Ebeoglugil, M.F.; Kayatekin, I.; Kutlu, B.; Culha, O.; Celik, E. Development of flame retardancy properties of new halogen-free phosphorous doped SiO_2 thin films on fabrics. *J. Appl. Polym. Sci.* **2007**, *105*, 3748–3756. [CrossRef]

29. Padovini, D.S.S.; Magdalena, A.G.; Capeli, R.G.; Longo, E.; Dalmaschio, C.J.; Chiquito, A.J.; Pontes, F.M. Synthesis and characterization of ZrO_2@SiO_2 core-shell nanostructure as nanocatalyst: Application for environmental remediation of rhodamine B dye aqueous solution. *Mater. Chem. Phys.* **2019**, *233*, 1–8. [CrossRef]

30. Puthai, W.; Kanezashi, M.; Nagasawa, H.; Tsuru, T. SiO_2-ZrO_2 nanofiltration membranes of different Si/Zr molar ratios: Stability in hot water and acid/alkaline solutions. *J. Membr. Sci.* **2017**, *524*, 700–711. [CrossRef]

31. Wang, H.; Li, G.; Xue, Y.; Li, L. Hydrated surface structure and its impacts on the stabilization of t-ZrO_2. *J. Solid State Chem.* **2007**, *180*, 2790–2797. [CrossRef]

32. Doğan, M.; Alkan, M.; Demirbaş, Ö.; Özdemir, Y.; Özmetin, C. Adsorption kinetics of maxilon blue GRL onto sepiolite from aqueous solutions. *Chem. Eng. J.* **2006**, *124*, 89–101. [CrossRef]

33. Mohammadnejad, M.; Hajiashrafi, T.; Rashnavadi, R. An erbium-organic framework as an adsorbent for the fast and selective adsorption of methylene blue from aqueous solutions. *Porous Mat.* **2017**, *25*, 761–769. [CrossRef]

34. Ahmed, M.J.; Islam, M.A.; Asif, M.; Hameed, B.H. Human hair-derived high surface area porous carbon material for the adsorption isotherm and kinetics of tetracycline antibiotics. *Bioresour. Technol.* **2017**, *243*, 778–784. [CrossRef]

35. Xiong, X.J.; Meng, X.J.; Zheng, T.L. Biosorption of C.I. Direct Blue 199 from aqueous solution by nonviable Aspergillus niger. *Hazard. Mater.* **2010**, *175*, 241–246. [CrossRef]

36. Otalvaro, J.O.; Avena, M.; Brigante, M. Adsorption of norfloxacin on a hexagonal mesoporous silica: Isotherms, kinetics and adsorbent reuse. *Adsorption* **2019**, *25*, 1375–1385. [CrossRef]

37. Liu, H.; Zhou, Y.; Yang, Y.; Zou, K.; Wu, R.; Xia, K.; Xie, S. Synthesis of polyethylenimine/graphene oxide for the adsorption of U(VI) from aqueous solution. *Appl. Surf. Sci.* **2019**, *471*, 88–95. [CrossRef]

38. Rani, S.; Mahajan, R.K. Equilibrium, kinetics and thermodynamic parameters for adsorptive removal of dye Basic Blue 9 by ground nut shells and Eichhornia. *Arab. J. Chem.* **2016**, *9*, S1464–S1477. [CrossRef]

39. Weber, T.W.; Chakravorti, R.K. Pore and solid diffusion models for fixed-bed adsorbers. *AIChE J.* **1974**, *20*, 228–238. [CrossRef]

40. Hall, K.R.; Eagleton, L.C.; Acrivos, A.; Vermeulen, T. Pore-and Solid-Diffusion Kinetics in Fixed-Bed Adsorption under Constant-Pattern Conditions. *Ind. Eng. Chem. Fundam.* **1966**, *5*, 212–223. [CrossRef]

41. Sherry, H.S.; Walton, H.F. The ion-exchange properties of zeolites. II. Ion exchange in the synthetic zeolite Linde 4A. *Phys. Chem.* **1967**, *71*, 1457–1465. [CrossRef]

42. Panneer, S.P.; Preethi, S.; Basakaralingam, P.; Thinakaran, N.; Sivasamy, A.; Sivanesan, S. Removal of rhodamine B from aqueous solution by adsorption onto sodium montmorillonite. *J. Hazard. Mater.* **2008**, *155*, 39–44.

43. Magdalena, P.K.; Joanna, G.; Robert, P. Removal of rhodamine B from water by modified carbon xerogels. *Colloids Surf. A Physicochem. Eng. Asp.* **2018**, *543*, 109–117.